Bottom Boundary Layer Structure and Detachment in the Shelfbreak Jet of the Middle Atlantic Bight*

ROBERT S. PICKART

Woods Hole Oceanographic Institution, Woods Hole, Massachusetts

(Manuscript received 11 August 1999, in final form 8 December 1999)

ABSTRACT

The hydrographic properties of the bottom boundary layer (BBL) are investigated in a synoptic cross section of the Middle Atlantic Bight shelfbreak frontal jet. The dataset consists of closely spaced conductivity–temperature–depth stations and concurrent shipboard acoustic Doppler current profiler measurements. An extremum in BBL properties occurs in the frontal region where the layer becomes thinner (disappearing briefly), more stratified, and more strongly capped. These changes are apparently related to the significant cross-slope variation in interior stratification. Where the BBL vanishes, at the shoreward edge of the front, it detaches into the interior along an (nearly) isopycnal layer. This is revealed both by weak vertical stratification as well as weak isopycnal gradients of potential temperature (θ) and salinity (S) along the layer. An advective–diffusive model of the detachment in density space is used to explain the observed θ, S distribution as well as estimate the pumping speed along the detached BBL. The detided ADCP velocity fields are analyzed in light of the observed detached BBL. The mechanism of detachment is discussed in relation to existing models, and the secondary circulation in the cross-stream plane is inferred. This reveals a deep interior upwelling cell, apparently tied to the local bathymetry, which enhances the flow along the detached BBL.

1. Introduction

The bottom boundary layer (BBL) is thought to play a fundamental role in the dynamics of stratified flow over sloping topography. In particular, near-bottom advection of buoyancy can have a profound effect on the character of the BBL and its impact on the interior flow field (e.g., Garrett et al. 1993). Downslope advection of light water beneath an equatorward-flowing boundary current can lead to lateral density gradients within the BBL that, via thermal wind, act to reduce the strength of the interior flow. In a steady state the bottom stress can be reduced to zero, in which case the interior flow is no longer retarded by bottom friction (Trowbridge and Lentz 1991; MacCready and Rhines 1993). A similar effect can occur for upslope advection beneath a poleward-flowing boundary current, though in this case the thermal wind adjustment takes place above a vanishingly thin BBL (Middleton and Ramsden 1996). Recently, Chapman and Lentz (1997) allowed for feedback between the interior flow and the evolving BBL, which extends these ideas to a plausible three-dimensional circulation. The observations of Trowbridge and Lentz (1998) offer the first quantitative evidence that such buoyancy-driven BBL dynamics may be at work in the ocean.

On the shelf, buoyancy advection by the BBL has been implicated in the establishment of a shelfbreak density front that spans the entire water column. Two related mechanisms have been put forth (see Fig. 1). Gawarkiewicz and Chapman (1992) investigated the spinup of a uniformly stratified equatorward shelf flow in which the BBL ultimately causes a lateral concentration of interior isopycnals. This in turn leads to a competing (upslope) pressure gradient in the BBL. The presence of a topographic shelfbreak enhances this effect to the point where the downslope flow in the BBL is arrested and the density front is subsequently ''trapped'' to the shelfbreak (Fig. 1a). In a separate study Chapman and Lentz (1994) addressed the formation of an analogous front due to an influx of buoyant (light) water into an unstratified equatorward shelf flow. In this case the geostrophic adjustment of the interior density front leads to poleward flow beneath (and seaward of) the shelf jet. The poleward flow in turn induces upslope flow in the BBL that counteracts the downslope flow shoreward of the front, and again the interior density front reaches an equilibrium position on the shelf (Fig.

* Woods Hole Oceanographic Institution Contribution Number 9965.

Corresponding author address: Dr. Robert S. Pickart, Woods Hole Oceanographic Institution, Woods Hole, MA 02543.
E-mail: rpickart@whoi.edu

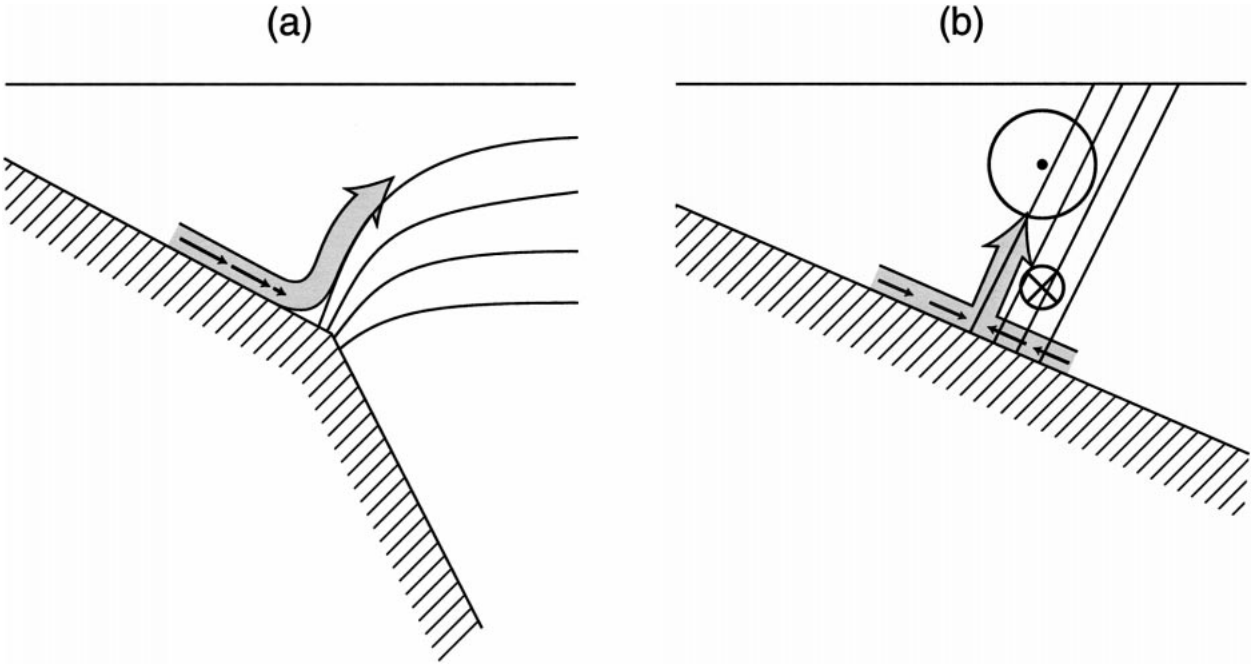

FIG. 1. Schematic of the shelfbreak front and detached BBL in two model studies. (a) Gawarkiewicz and Chapman (1992) model: convergent flow in the BBL (short arrows) detaches at the shelfbreak due to the onshore pressure gradient resulting from the concentration of frontal isopycnals. The large shaded arrow denotes the trajectories of fluid parcels as they advect into the interior. (b) Chapman and Lentz (1994) model: Geostrophic adjustment of the front leads to a flow reversal in the jet at depth ($\odot$: equatorward flow, $\otimes$: poleward flow), which leads to opposing upslope and downslope flow in the BBL; the associated collision leads to detachment.

1b). A characteristic common to both of the above solutions is the so-called detachment of the BBL. Because downslope flow in the BBL is blocked at the front—due to the competing pressure gradient in the Gawarkiewicz and Chapman (1992) model and the upslope BBL flow in the Chapman and Lentz (1994) model—water parcels are forced out of the BBL into the interior of the water column (Fig. 1).

These ideas may be relevant to the shelfbreak front of the Middle Atlantic Bight. This front, separating cold, fresh shelf water from warm, salty slope water, is associated with an equatorward jet on the order of 25 cm s^{-1} (e.g., Linder and Gawarkiewicz 1998). This current is believed to be the subtropical extension of the Labrador Current (Loder et al. 1998). A recent dye-release experiment at the bottom of the shelfbreak front near 70°W (Houghton and Visbeck 1998) beautifully demonstrated the detachment of water parcels from the BBL along an interior isopycnal. Distributions of suspended sediments in the region also imply such a detachment (Barth et al. 1998). These measurements are the first documentation of the detachment process, and lend encouraging support to some of the modeling results to date. Intriguing as they are, however, the observations are largely suggestive; furthermore they were difficult to obtain (requiring the use of special tracers). Clearly, additional measurements of the BBL and its detachment are required to help quantify the dynamics at work in the Middle Atlantic Bight shelfbreak system; it is also of value to devise easier ways to reveal such processes using more conventional data. This is the motivation for the present study.

In this analysis a single synoptic hydrographic section is used to investigate the characteristics of the BBL associated with the shelfbreak jet near 70°W. The cross-stream structure of the BBL so revealed can be related to the overlying interior flow. Detachment of the BBL near the foot of the front is clearly evident in the hydrographic data, and is mapped out using two independent techniques. The first method detects the detached layer via a local minimum in vertical stratification, while the second method uses reduced lateral gradients of potential temperature and salinity resulting from advection along the layer. A simple advective–diffusive numerical model is developed to explain this distribution of properties along isopycnals and is used to estimate the pumping velocity along the detached BBL. Finally, the synoptic, detided velocity fields from the shipboard acoustic Doppler current profiler are examined in the context of the detached BBL, and are used to elucidate the secondary circulation.

2. Dataset

In May of 1996 a conductivity–temperature–depth (CTD) section was occupied across the shelfbreak jet near 70°W (Fig. 2). This is one of a series of such hydrographic sections obtained along TOPEX altimetric

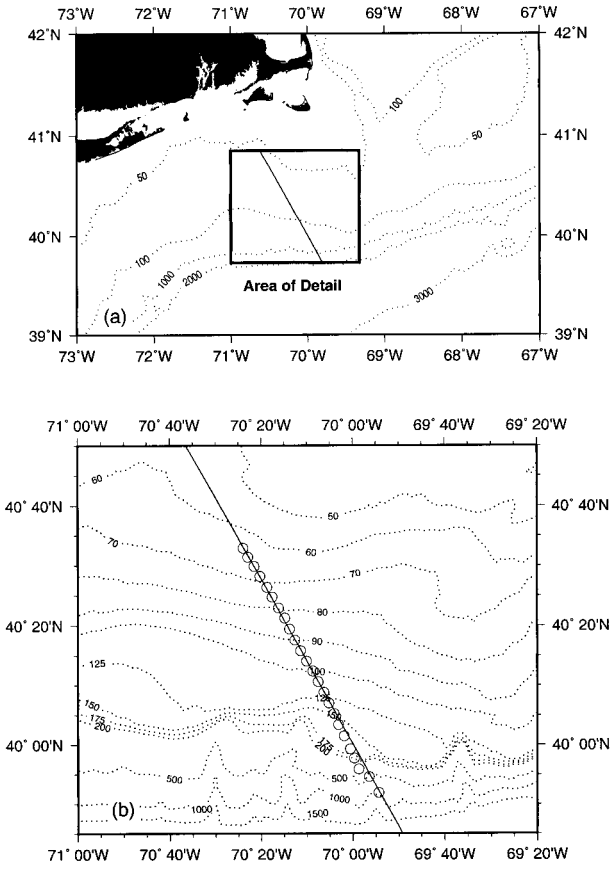

FIG. 2. (a) Domain of the Shelfbreak PRIMER experiment in the Middle Atlantic Bight. The solid line is the TOPEX altimetric subtrack. (b) Detailed view showing the locations of the CTD stations (circles) comprising the May 1996 section.

subtrack C126 as part of the Shelfbreak PRIMER experiment between 1995–97. PRIMER is a joint acoustics/physical oceanography study of the shelfbreak front and adjacent slope water in the Middle Atlantic Bight [see Pickart et al. (1999) for a more detailed description of the experiment]. Two earlier occupations of the TOPEX CTD line were reported on by Pickart et al. (1999) in a study of meander characteristics of the jet. The May 1996 section was chosen for the present BBL analysis because concurrent SeaSoar data from the frontal region were being analyzed simultaneously by other PRIMER investigators (see Gawarkiewicz et al. 1999, manuscript submitted to *J. Phys. Oceanogr.*).

The CTD section consists of 23 stations spaced 3.7 km apart occupied over a 15-h period (with an additional station taken two hours later, 6 km farther offshore). A Neil Brown Instrument Systems Mark-III CTD was used, calibrated in the laboratory and checked using a small number of in situ salinity samples. The accuracy in temperature is 0.001°C, and in salinity is 0.02 psu. In the present analysis the data were used both in 2-db averaged form and in individual scan form (i.e., calibrated but not pressure averaged). Although considerably noisier, the individual scan data provide high vertical resolution, which was necessary for unambiguously detecting the BBL. It is clearly stated throughout the paper when the individual scan data are used versus the pressure-averaged data.

Shipboard acoustic Doppler current profiler (ADCP) data were also collected along the section, with cross-stream resolution of 250 m and vertical resolution of 8 m. The reader is referred to Pickart et al. (1999) for a description of the processing and calibration of the ADCP data, including an analysis of the errors involved. The major difference between this study and Pickart et al. (1999) is that the velocity data here have been corrected for the barotropic tide using the scheme developed by Fratantoni et al. (1999, manuscript submitted to *J. Phys. Oceanogr.*, hereafter FPTS), which makes use of moored data along the TOPEX line. Fratantoni et al. also demonstrated that the baroclinic tide in this region is negligible compared to the barotropic tide, and hence is not a significant source of error. The strength of the inertial oscillations can be estimated using the moored ADCP data collected during the PRIMER experiment (FTPS). In the vicinity of the jet the inertial amplitudes were 3–4 cm s^{-1} during the time of the section, much less than the alongstream and cross-stream velocity signals of interest (see section 6). The synoptic ADCP fields presented here are thus an accurate measure of the subtidal flow associated with the shelfbreak jet.

The shelfbreak front is clearly evident in the vertical sections (Fig. 3) of potential temperature (θ), salinity (S), and potential density (σ_θ). Note the beginnings of the seasonal thermocline in the upper 20–30 m and the associated cold pool beneath it inshore of the front. This is typical of midspring conditions [the near-surface stratification is maximum in August; see Linder and Gawarkiewicz (1998)]. Two features of note in the sections, which have bearing on the shelfbreak jet and BBL, are the shoreward extension of the foot of the front (near 75 km) and the ''mini''-shelfbreak near 105 km (the shelfbreak proper is located near 125 km at a depth of 160 m).

3. Bottom boundary layer structure

To date there have been no observations characterizing the hydrographic structure of the BBL across the shelfbreak jet of the Middle Atlantic Bight. It is worth noting as well that the main purpose of the section presented here was to sample the jet, not to investigate the BBL. However, during the cruise the instrument package was generally lowered to within 3–5 m of the bottom, which almost always penetrated the BBL. Thus, even though CTD measurements of this sort are not ideal for such a study, the lack of historical BBL information beneath the jet provided a compelling reason to pursue this investigation.

In the present study the BBL is defined as the weakly

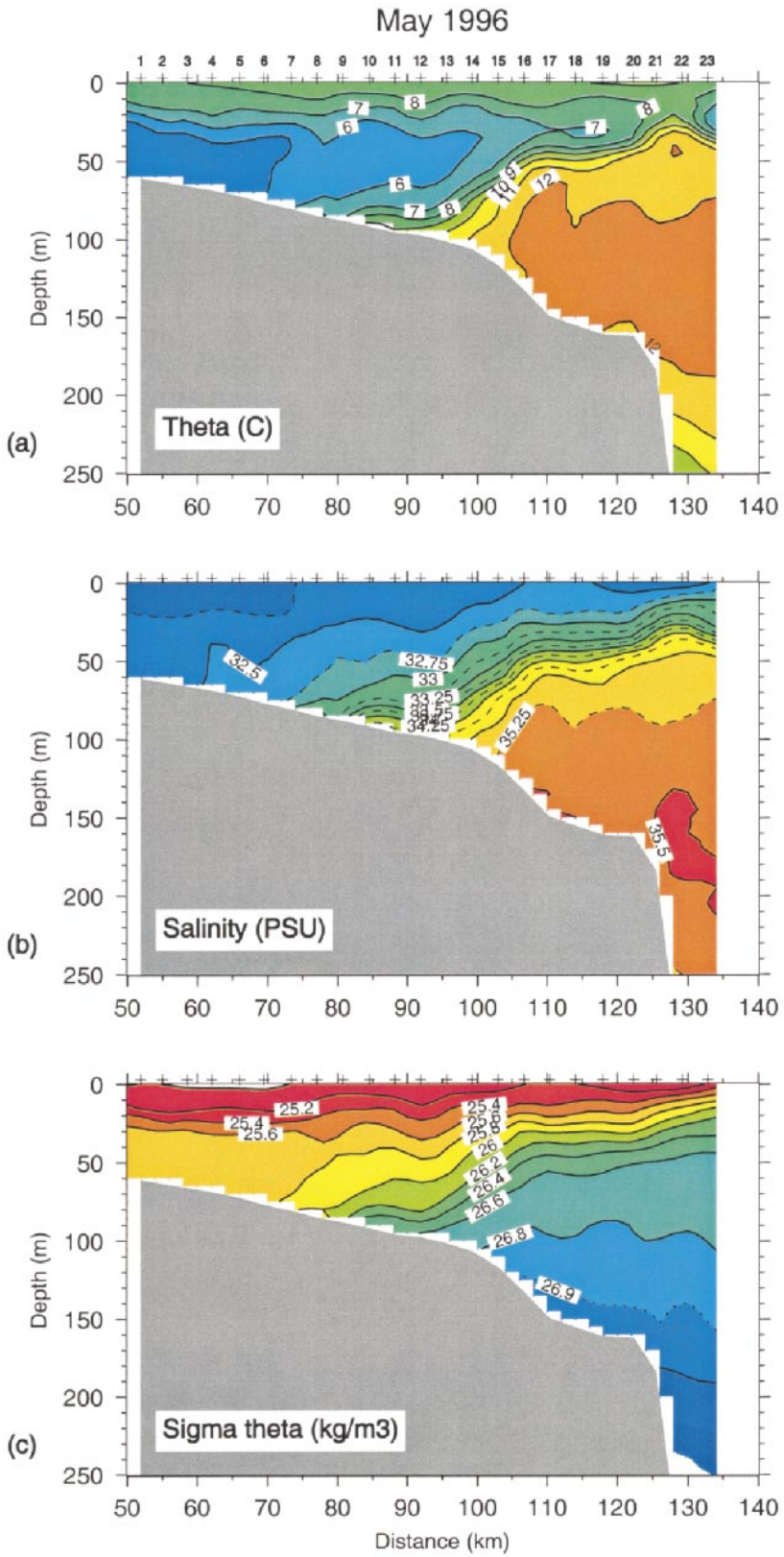

FIG. 3. Vertical sections of (a) potential temperature, (b) salinity, and (c) potential density.

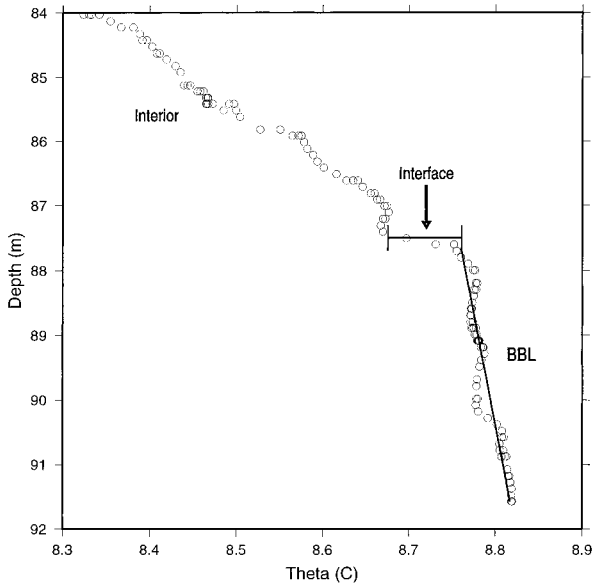

FIG. 4. Near-bottom profile of potential temperature at station 11 (the data have been subsampled for presentation). The polynomial fit to the BBL is shown, and the change in temperature, $\Delta\theta$, across the upper interface of the BBL is marked as well.

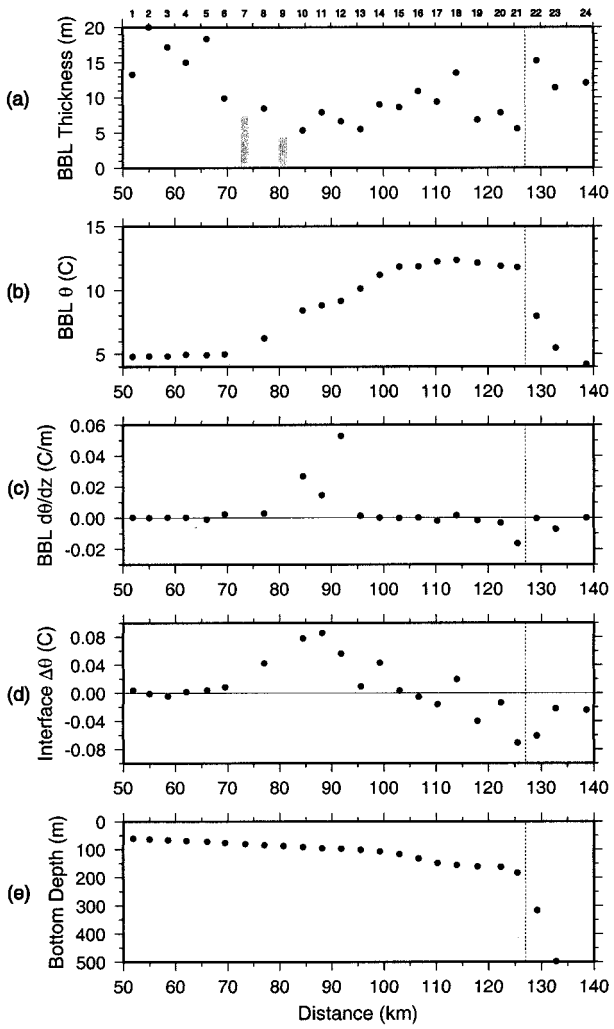

FIG. 5. Hydrographic properties of the BBL from the PRIMER CTD section. There are two stations, 7 and 9, where a BBL was not observed; the maximum depth of the CTD package at these two sites is indicated by the grey lines. The dashed line marks the location of the shelfbreak.

stratified near-bottom layer, which is separated from the (more strongly stratified) interior by a distinct interface in temperature, salinity, and density (Fig. 4). Interestingly, at none of the sites was this layer truly unstratified. This is in contrast, for example, to the uniform boundary layer observed beneath the deep western boundary current by Stahr and Sanford (1999). Although varying degrees of weak BBL stratification were observed in the PRIMER section, in each instance the property gradients (T, S, σ_θ) were significantly nonzero relative to the accuracy of the CTD (which was calibrated to deep water standards). Only the BBL temperature data are presented here since the CTD thermistor was less noisy than the conductivity sensor; however, both salinity and density show the same features.

The deep portion of every CTD station was examined in detail using the individual scan data. In all but two of the stations a BBL, defined as above, was detected. A linear polynomial was fit to the portion of the BBL measured by the CTD, then extrapolated to the seafloor (Fig. 4). The bottom depth at each site was determined by knowing the depth of the deepest measurement and the height of the instrument package above the bottom via the line-scan recorder. Note that this analysis determines only the gross characteristics of the BBL and obviously ignores the detailed structure as one approaches the solid boundary.

A surprisingly consistent pattern emerges when one examines the cross-stream structure of the BBL based on the above polynomial fits (Fig. 5). Shoreward of the shelfbreak front the BBL is thick (order 15–20 m), nearly unstratified, and separated from the interior by a weak interface. By contrast, in the vicinity of the shelfbreak front (centered near 90 km) the BBL thins considerably (order 5–7 m), is significantly stratified, and is bounded above by a strong interface. Seaward of the front the BBL once again thickens and becomes more reminiscent of that found on the shelf. The existence of the density interface above the BBL suggests that the BBL itself may be largely the result of mechanical mixing rather than convective overturning, simply because near-bottom stirring of an initially varying profile would result in such a property jump. This is consistent with the low Richardson numbers measured by Houghton and Visbeck (1998) within the BBL. Such a density jump violates the assumption made by Trowbridge and Lentz (1991) in developing their steady state one-dimensional BBL model.

It is of interest to try and explain the observed ex-

trema in BBL properties associated with the shelfbreak front (i.e., the minimum in thickness, maximum in stratification). Trowbridge and Lentz (1991) present a relationship for BBL thickness as a function of the interior flow parameters, for the case of downslope Ekman flow (equatorward jet). Inherent in their result is the assumption that the interior flow is not impacted by the BBL. Chapman and Lentz (1997) later modified this relationship by allowing for feedback between the BBL and interior. Chapman and Lentz's (1997) scale estimate for the BBL height is

$$h_{\max} \sim \sqrt{f\mathcal{T}/N^2}, \tag{1}$$

where $h_{\max}$ is the BBL thickness scale, $\mathcal{T}$ is the transport per unit depth of the jet, f is the Coriolis parameter, and N is the (constant) stratification of the interior. Interestingly, the bottom slope does not appear in (1), but does appear in Trowbridge and Lentz's (1991) result; this is due to the fact that the interior flow is allowed to adjust to the BBL in the Chapman and Lentz (1997) model.

The interior flow characteristics observed in the PRIMER hydrographic section are shown in relation to the BBL thickness in Fig. 6. Not surprisingly there is a large increase in interior stratification (associated with the shelfbreak front) coinciding with the deep equatorward jet, both of which are aligned with the local minimum in BBL thickness. The bottom slope (obtained from the vessel-mounted chirp sonar) shows the mini-shelfbreak just seaward of this. One is tempted to think that both the interior stratification and jet peak bear on the small observed BBL. According to (1), however, stronger equatorward flow should produce a larger BBL height. This suggests that it is the horizontally varying interior stratification that causes the sharp change in BBL characteristics. Interestingly, using representative values (taken from Fig. 6) for the parameters in Eq. (1), the BBL scale height so predicted is an order of magnitude too large. This is likely due to the assumption of flat interior isopycnals in the Chapman and Lentz (1997) model, a notion that deserves further study.

Just inshore of the shelfbreak proper the BBL thins a second time, again with a tendency for increased stratification and a stronger bounding interface (the sense of the temperature change across the interface is now opposite, that is, warm water above cold, Fig. 5). On the other side of the shelfbreak the BBL reverts back as before. There are at least two possible factors that may have bearing on this temporary change in properties—bottom slope and slope water influence. Note that this location is characterized by a minimum in bottom slope (i.e., in between the mini-shelfbreak and shelfbreak proper, Fig. 6d). In addition, residing on this plateau is a near-bottom pool of cold, fresh slope water (e.g., colder than 12°C at station 20, Fig. 3a). While it is unclear as to which of these factors might lead to the observed change in BBL properties (these factors may be related), it does implicate the importance of local bottom topography, as well as the ambient slope water, in the dynamics of the BBL.

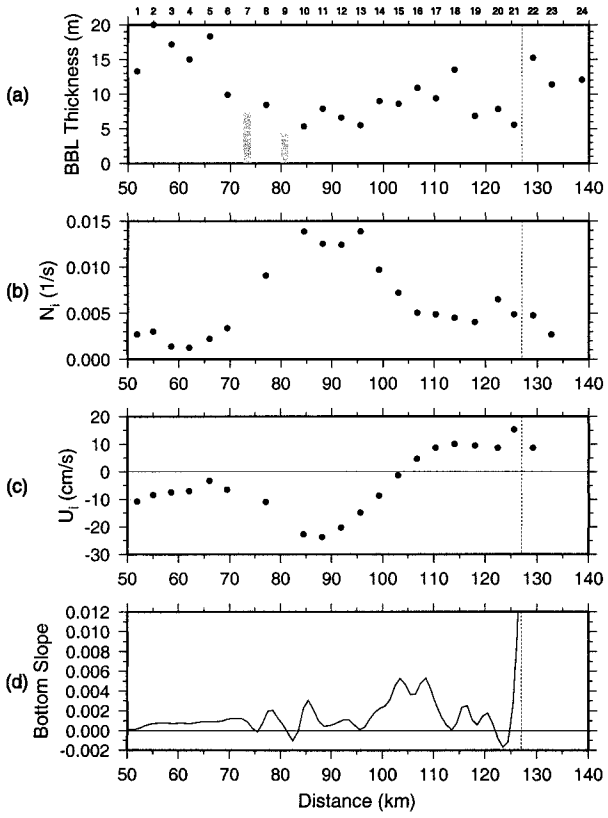

FIG. 6. Properties of the interior flow—buoyancy frequency (N_i), alongstream velocity (U_i), and bottom slope—in relation to the BBL thickness. The interior values are averaged over the bottom 30 m of the water column, excluding the BBL (this includes extrapolated portions of the along-stream velocity of the jet, see section 6b). The dashed line marks the location of the shelfbreak.

4. Detachment of the bottom boundary layer

Previous modeling work has suggested that the downslope flow in the BBL beneath the equatorward-flowing shelfbreak jet should separate from the bottom upon encountering the shelfbreak front. This process was elucidated via Lagrangian particle tracking by both Gawarkiewicz and Chapman (1992) and Chapman and Lentz (1994). Recent observations near the PRIMER site have documented such a detachment process in the Middle Atlantic Bight shelfbreak jet. A dye-release near the foot of the front has clearly depicted water parcels advecting from the BBL into the interior along an isopycnal (Houghton and Visbeck 1998). Barth et al. (1998) present complementary evidence using the distribution of suspended sediments. These results motivate one to look for signs of BBL detachment in the physical θ, S data. This could potentially shed much light on the processes involved, and hydrographic data are consid-

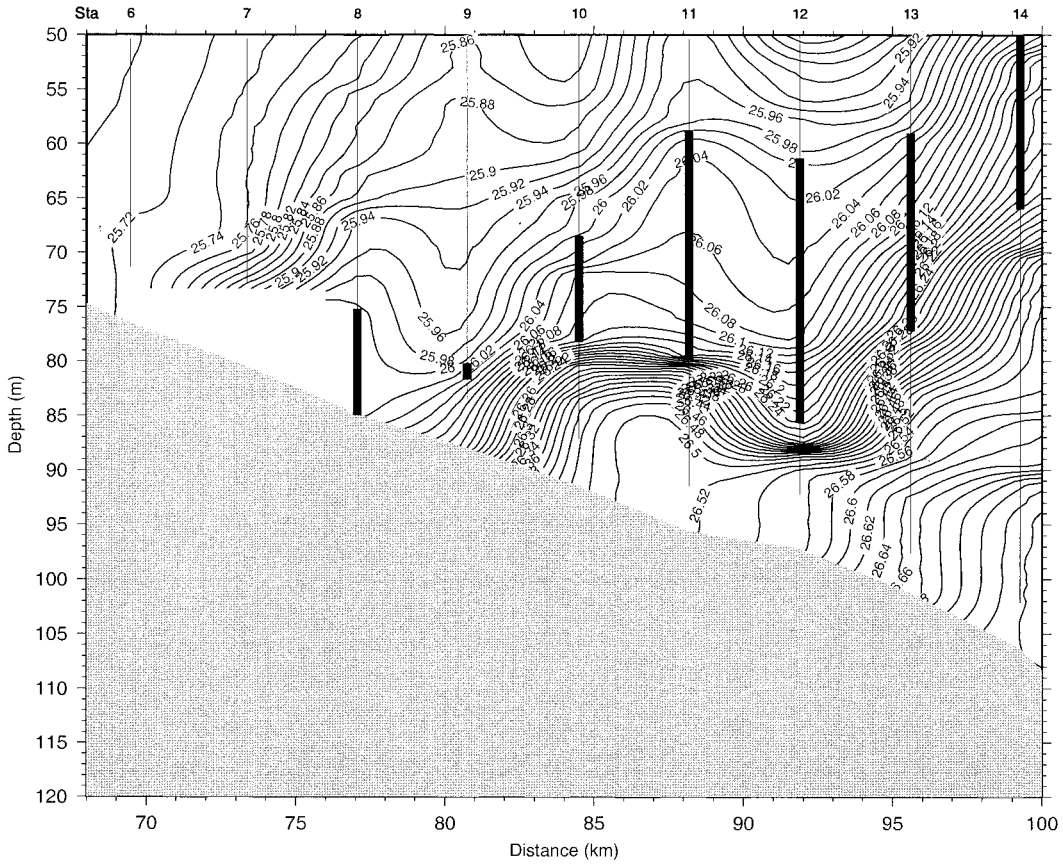

FIG. 7. Potential density near the foot of the front (σ_θ in kg m^{-3}). The solid dark lines denote the layer of weak vertical stratification at each station, as discussed in the text. The thin lines mark the CTD traces (no extrapolation was done for station 7 because the instrument package was stopped anomalously far above the bottom). Note that to make this contour plot the raw scan data were decimated, gridded, and slightly smoothed, hence the plot does not perfectly resolve the interfaces of the BBL and detached BBL.

erably easier to obtain than dye-release observations or other measurements of special tracers.

a. Vertical stratification

As mentioned above there were two stations in the PRIMER CTD section where a BBL was not detected; both of these were located near the shoreward edge of the shelfbreak front (Fig. 5a). The lack of a BBL at the shallower site may have been due to the fact that the CTD was stopped anomalously far above the bottom (i.e., the instrument may not have penetrated the BBL). However, this is likely not the case at the deeper station where the CTD was lowered to 4.4 m above the seafloor. The disappearance of the BBL at this site suggests that detachment may be occurring here.

Recall that the BBL is a weakly stratified layer bounded above by a distinct interface (Fig. 4); moving offshore, the layer becomes progressively more dense. At the last station prior to the disappearance of the BBL, the upper interface occurs at $\sigma_\theta = 26.0$ (station 8, Fig. 7). If parcels in the layer are detaching near this site, one might expect to see the remnant of weak stratification, as well as the upper interface, in succeeding stations. The individual CTD scan data were closely examined for such evidence, which was readily apparent. In particular, a distinct density interface is identifiable near $\sigma_\theta = 26.0$, which delineates a layer of weak stratification bounded below by the shelfbreak front (Fig. 8). The layer defined as such is shown in Fig. 7; this presumably maps out the detached BBL as it separates off the bottom adjacent to the foot of the shelfbreak front.

Note the variation in thickness of the detached layer from station to station; this is likely due to the deformation of the local density surfaces by internal waves. Despite the significant amplitude of such waves, however, the weakly stratified layer persists—albeit becoming more stratified as it extends seaward. It is important to realize that the density interface at $\sigma_\theta = 26.0$ is often so sharp that it does not appear in the 2-db averaged CTD data; not until the individual scan data were used did the detached BBL become evident. This may be considered a limitation of this technique, since it is

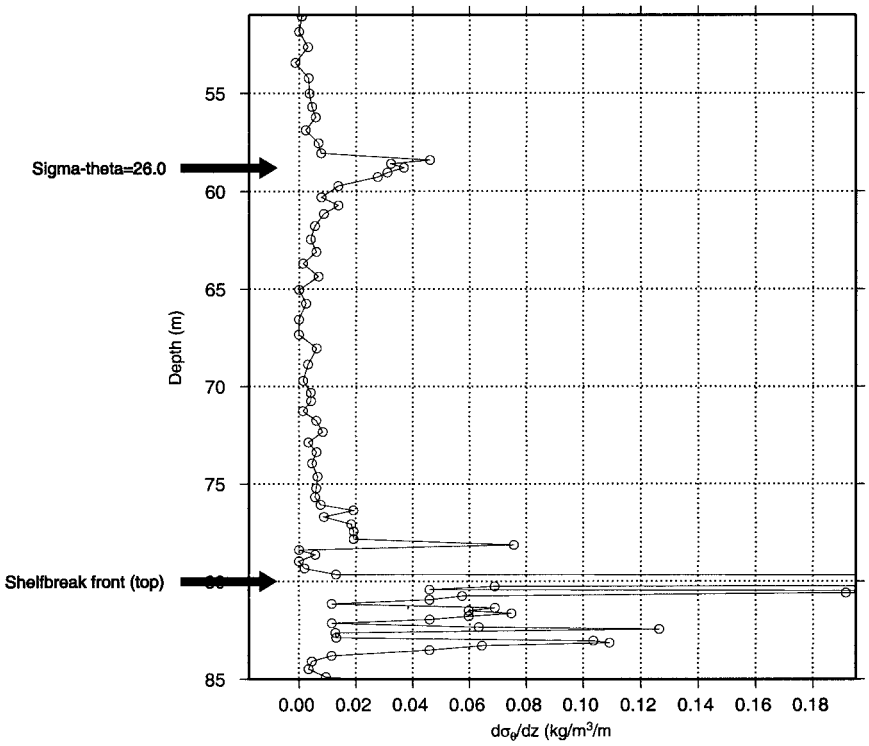

FIG. 8. Vertical density gradient at station 11, showing the peaks of increased stratification which define the top and bottom of the detached BBL (the data have been subsampled for presentation).

somewhat cumbersome to work with individual scan data and such data may not be available for historical sections.

b. Isopycnal analysis

Progressing from onshore to offshore along the isopycnals of the shelfbreak front, they become warmer and saltier; that is, the shelfbreak front is a temperature and salinity front in density space as well. Hence one expects there to be significant along-isopycnal mixing in this region. Now if water parcels are being pumped along the (nearly isopycnal) layer depicted in Fig. 7, then one might expect to see reduced lateral gradients of θ and S along this layer, relative to the adjacent isopycnal surfaces above and below where there is no such advection. In other words, the advection would weaken the gradients that are otherwise there in the presence of isopycnal mixing. To see if this is the case, the PRIMER potential temperature section was plotted in density space (Fig. 9). A scaled depth coordinate (z') was used, which was defined using the mean depth–density relationship for the entire collection of CTD stations (see also Pickart and Smethie 1998). Both the cold pool (centered near 90 km) and the shelfbreak temperature front are clearly evident in the figure.

Next a section of $d\theta/dy$ was constructed (where the gradient is along isopycnals in the offshore direction), which to first order is dominated by the temperature ''wiggles'' seen in Fig. 9 (e.g., follow the 8°C contour). There is no simple explanation for these undulations, which are surprisingly coherent with depth. Nonetheless, a clear region of minimum $d\theta/dy$ is evident near $\sigma_\theta = 26.0$ (not shown). This is not surprising in light of the tongue formed by the 7°C contour at this density (Fig. 9). Finally, to present things in the clearest possible fashion, a section of ''accumulated temperature change'' was constructed by simply integrating $|d\theta/dy|$ along each isopycnal, starting with a temperature of zero at the bottom (then transforming the section back to the familiar depth-distance coordinate frame). This reveals a distinct tongue of minimum accumulated temperature change, which coincides exactly with the layer of minimum vertical stratification determined above (Fig. 10). Clearly this is the signature of the detached BBL.

It is important to realize that this method does not involve use of the individual CTD scan data; Fig. 10 was constructed using 2-db averaged data. Thus the calculation of accumulated temperature change represents a relatively easy method to identify the path of the detached BBL using basic physical data. This has important ramifications. For instance, it means that complex procedures such as a dye release or use of special tracers are not the only means to obtain information on the detached BBL. Furthermore, this method can be applied to any historical CTD section. As noted above, the

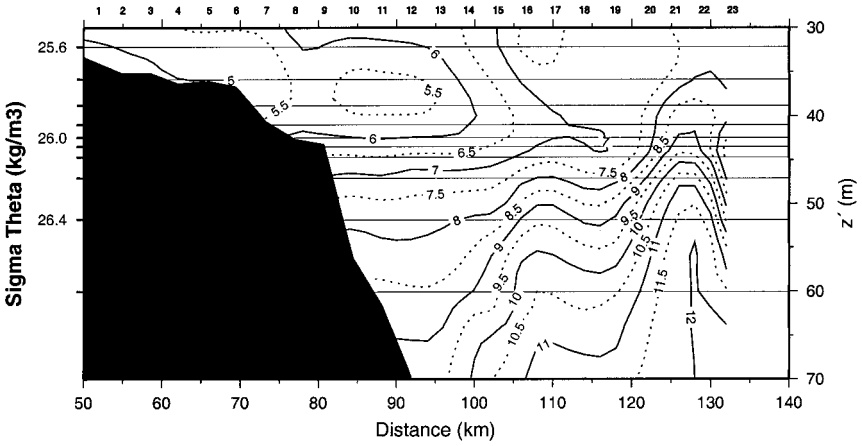

FIG. 9. Vertical section of potential temperature (°C) constructed in density space.

PRIMER experiment included detailed three-dimensional mapping of the shelfbreak front using SeaSoar. A brief SeaSoar test cruise, conducted shortly after the TOPEX CTD line was occupied, resulted in four high-resolution cross sections of the front and jet (Gawarkiewicz et al. 1999, submitted to *J. Phys. Oceanogr.*). Sections of accumulated temperature change were computed using these data, and in each case the detached BBL was clearly evident as it is in Fig. 10. It is planned to apply this technique to the PRIMER summertime and wintertime SeaSaor datasets, which are weeklong reoccupations of a set of frontal cross sections. This will help elucidate the space/time evolution of the detached BBL and its interaction with the shelfbreak jet, including any seasonal differences.

5. Advective–diffusive model of detachment

In order to help interpret the tongue of minimum accumulated temperature change in Fig. 10, as well as estimate the magnitude of the pumping along the detached BBL, a simple advective–diffusive numerical model of the front was developed. The model is formulated in density space (specifically in the scaled vertical coordinate z') and is used to investigate the effect of advection along an isopycnal in the presence of the shelfbreak temperature front (Fig. 11). The region of inflow corresponds to the detached BBL, and the left and right boundaries of the model correspond to the shoreward (cold) and seaward (warm) sides of the front. This configuration is meant to represent the vertical potential temperature section in density space, that is, Fig. 9 (without the undulations). The steady-state two-dimensional advective–diffusive balance is sought.

The governing equation is

$$v(z')\frac{\partial\theta}{\partial y} = \kappa_h\frac{\partial^2\theta}{\partial y^2} + \kappa_v\frac{\partial^2\theta}{\partial z'^2}, \tag{2}$$

where y is cross-stream distance (positive offshore), z' is scaled depth (positive upward), θ is potential temperature, κ_h and κ_v are the isopycnal and diapycnal diffusivities, and $v(z')$ is the speed of parcels along the detached BBL. For boundary conditions, the change in potential temperature across the front (ΔT_y) is specified, along with the top to bottom change in temperature ($\Delta T_{z'}$), where these are estimated from the data (i.e., the average frontal slope from Fig. 9). The final boundary condition is no-flux at the top and bottom boundaries, $\theta_{z'} = 0$.

To obtain a solution, (2) was integrated vertically and the domain was represented as a series of isopycnal layers (of width Δh), each layer depicted by a single value of temperature. Within each layer a finite-difference approximation was applied laterally (grid spacing of Δy), resulting in the following equation for an interior isopycnal,

$$\theta_{i+1}^j - (2R + P + 2)\theta_i^j + (P + 1)\theta_{i-1}^j + R\theta_i^{j-1} + R\theta_i^{j+1} = 0, \tag{3}$$

where $P = V\Delta y/\kappa_h$ is the Peclet number, and $R = \kappa_v\Delta y^2/\kappa_h\Delta h^2$ is a measure of the relative importance of diapycnal versus isopycnal mixing. Note that P is nonzero only for those isopycnals comprising the detached BBL, where V is the constant advective speed along these isopycnals (see Fig. 11). The system of equations for the complete range of i and j can be solved in matrix form using standard singular value decomposition. The model resolution used was 2 km in the horizontal, and 35 density layers (the detached BBL was represented by three layers, as suggested from the data).

a. Model solutions: Dependence on parameters

The free parameters in the model are the isopycnal and diapycnal diffusivities, κ_h and κ_v, and the pumping speed along the detached BBL, V. The steady-state advective–diffusive balance is shown in Figs. 12a–d for several different choices of these parameters, in order

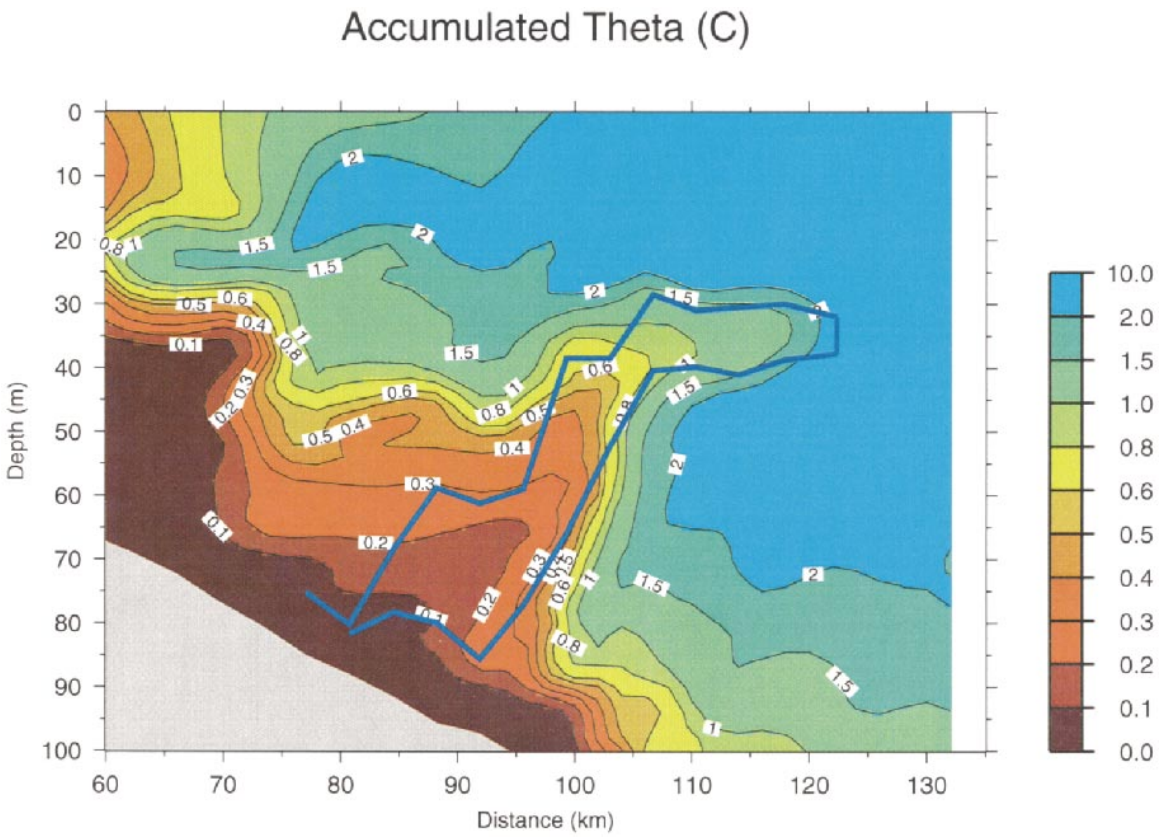

FIG. 10. Section of accumulated temperature change as defined in the text. Overlayed on this is the layer of weak vertical stratification (delineated by the dark blue line).

to elucidate the character of the solution and how it is altered when the mixing and advection are changed. In each case both the temperature is shown, as well as the accumulated temperature change as defined above. Only the middle 15 density layers are displayed.

In the first case (Fig. 12a) there is no vertical mixing or advection, and the isotherms are uniformly sloped in accordance with the lateral boundary conditions. The second case (Fig. 12b) has moderate vertical mixing and a pumping speed of 1 cm s^{-1}. Note that with such weak advection the isotherms are only slightly distorted from

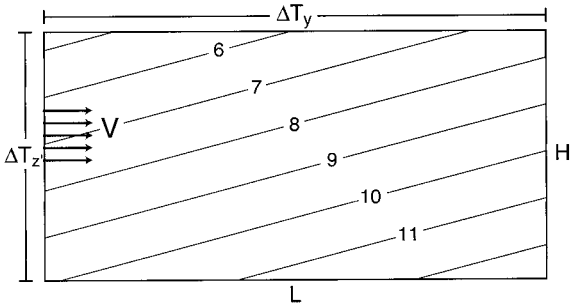

FIG. 11. Schematic of the numerical model domain, indicating the region of inflow (V) and boundary conditions.

their ''equilibrium'' position of the previous case, yet the accumulated temperature change shows a marked tongue clearly revealing the detached BBL. This demonstrates the effectiveness of using accumulated temperature change as a tracer. Recall that the CTD potential temperature section in density space showed undulations not related to the detached BBL, just as any such data will contain a fair amount of noise, making it difficult to recognize more subtle effects that may be due to the detachment process.

The third example (Fig. 12c) shows a case with strong advection in which the tongue of accumulated temperature change is extremely pronounced (in fact the isotherms themselves form a weak tongue over part of the domain). This shows nicely the sensitivity of the solution to the magnitude of the pumping, the only change between this case and the previous one being an increase in advection from 1 to 5 cm s^{-1}. It also suggests that the model could indeed be effective in characterizing the observed tongue of Fig. 10 in terms of pumping speed. The final example is one in which the vertical diffusivity is set quite high (once again with weak advection, Fig. 12d). In this case there is no noticeable tongue in accumulated temperature change, while the isotherms themselves still display a distribution indic-

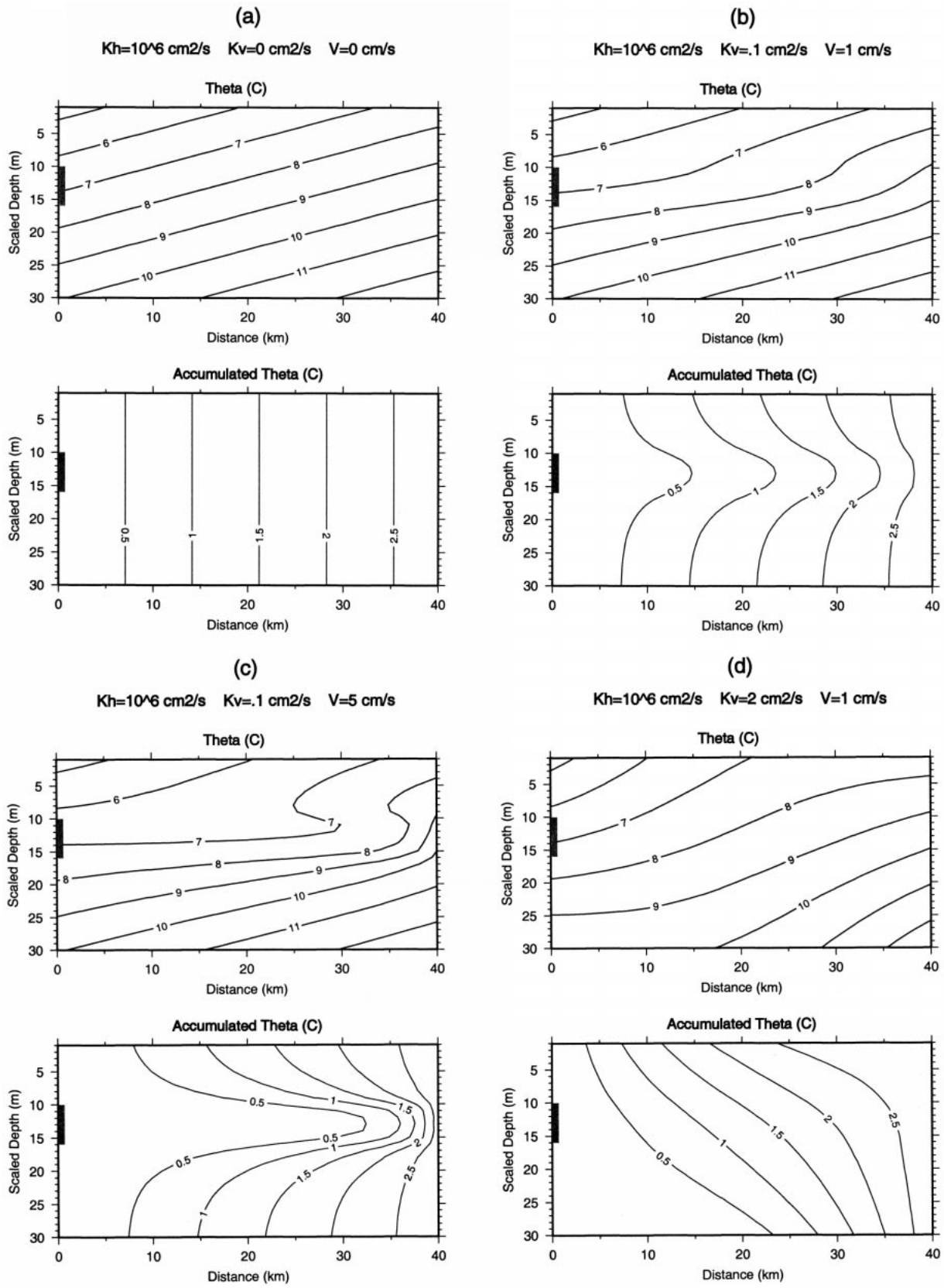

FIG. 12. Solutions of the advective-diffusive model for different values of the diapycnal mixing and pumping speed. The gray line marks the region of inflow.

ative of a shelfbreak front. In the limit of unrealistically large vertical diffusivity (not shown) the shelfbreak frontal isotherms become completely vertical, except for immediately adjacent to the lateral boundaries.

b. Model/data comparison: Estimated pumping speed

The numerical model is now used to estimate the magnitude of the flow along the detached BBL that would cause the observed distribution of accumulated temperature change in Fig. 10. Of the three parameters in the model, the most is known about the diapycnal diffusivity κ_v. Coinciding with the PRIMER study was a separate experiment, Coastal Mixing and Optics (CMO), undertaken in the same general vicinity of the shelf and shelfbreak in the Middle Atlantic Bight. As part of CMO microstructure measurements were conducted (Rehmann and Duda 2000), which produced estimates of κ_v. Hence the approach taken here is that κ_v is a known parameter (with uncertainties of course), and the model is then tuned to the data providing an estimate of the pumping speed V and isopycnal diffusivity κ_h.

From the data, the along-isopycnal distribution of accumulated temperature change was determined (over the half-width of the tongue in Fig. 10), as well as the vertical distribution (averaged across-stream). Tuning the model solution to the data then involves optimizing the fit of accumulated temperature change in both of these directions—in particular, minimizing the rms difference between the model and data tongue distributions in both y and z'. This was accomplished as follows. For a given value of κ_v, the other two parameters were systematically varied over two orders of magnitude. A contour plot of rms difference readily identifies the (V, κ_h) pair that results in the best fit to the data as described above. This was then repeated for different values of κ_v over a range of values guided by the CMO data.

The rms fits for two of the choices of diapycnal diffusivity are shown in Fig. 13. A clear rms minimum appears for both the y fit and the z' fit, but note that the optimal (V, κ_h) pair for the separate fits is not quite the same. It is clear, however, from the overall distribution (which minimizes the vector rms fit) that the z' distribution provides the biggest constraint on the model. In other words, the cross-isopycnal spread of the accumulated tracer tongue is most sensitive to variation in the parameters. When the diapycnal diffusivity is decreased, the associated optimal value of V and κ_h decrease as well (compare Figs. 13a to 13b). However, the magnitude of the rms minimum in each case is the same. This is because the model solution is, in fact, identical for certain combinations of the parameters. Hence, it is crucial to have the independent information about the diapycnal diffusivity; that is, without the CMO estimates of κ_v the model could not be used to estimate the pumping speed of the detached BBL.

The locus of optimal (V, κ_h) pairs for the range of diapycnal diffusivities considered reveals a clear linear relationship between the magnitude of the best-fit pumping speed and isopycnal mixing (not shown). Assuming such a straight line fit, Fig. 14 shows the predicted value of V and κ_h for the PRIMER CTD section as a function of κ_v. Which (V, κ_h) pair is the best one? This of course depends on determining the most realistic value of κ_v. The microstructure measurements during CMO produced estimates of κ_v as a function of buoyancy frequency, which are dependent as well on the magnitude of the Turner angle (Rehmann and Duda 2000). The Turner angle measures the sensitivity of a parcel of water to double-diffusive instability and depicts three different possible regimes: salt fingering, diffusive layering, or diffusively stable. The calculated Turner angle for the PRIMER hydrographic section indicates that the detached BBL lies mostly within the diffusive-layering regime (characterized by cold, fresh over warm, salty water). The average calculated buoyancy frequency along the detached BBL is 8 cph.[1]

Using the values of κ_v from Rehmann and Duda (2000), for the diffusive-layering regime, suggests a value of $\kappa_v \sim 0.25$ cm^2 s^{-1} for the calculated buoyancy frequency (Fig. 15). This in turn implies a pumping speed of 3.7 cm s^{-1} along the detached BBL and an isopycnal diffusivity of 1.6 cm^2 s^{-1} (Fig. 14). These values should be considered the best model prediction based on the observed distribution of accumulated temperature change (the model and data fields in fact agree quite well, Fig. 16). This value of V is somewhat larger than the pumping speed of 2 cm s^{-1} determined directly from the near-bottom dye release of Houghton and Visbeck (1998). Using the average isopycnal slope of the detached BBL in Fig. 3c, the present estimate converts to a vertical velocity of 9 m day^{-1}, which is quite close to that estimated by Barth et al. (1998). The value presented here is of course only as good as the estimate for diapycnal mixing. While there is a clear trend in κ_v versus buoyancy frequency from the microstructure measurements (Fig. 15), there is also significant scatter; thus one should consider the entire range of pumping speeds shown in Fig. 14 as viable possibilities. In fact, estimates from dye dispersion studies during CMO (inshore of the detached BBL) are generally of order $\kappa_v \sim 0.05$ cm^2 s^{-1} for buoyancy frequency ranging from 8 to 20 cph (J. Ledwell 1999, personal communication).

[1] As the BBL detaches and extends into the interior it forms a tongue of minimum buoyancy frequency (calculated from the 2-db data) much like the temperature tongue delineated by the 7°C isotherm pointed out earlier (see Fig. 3a). These extrema in properties (whose significance might easily have gone unnoticed) extend to within 30 m of the sea surface—yet remarkably they are the consequence of bottom boundary layer dynamics.

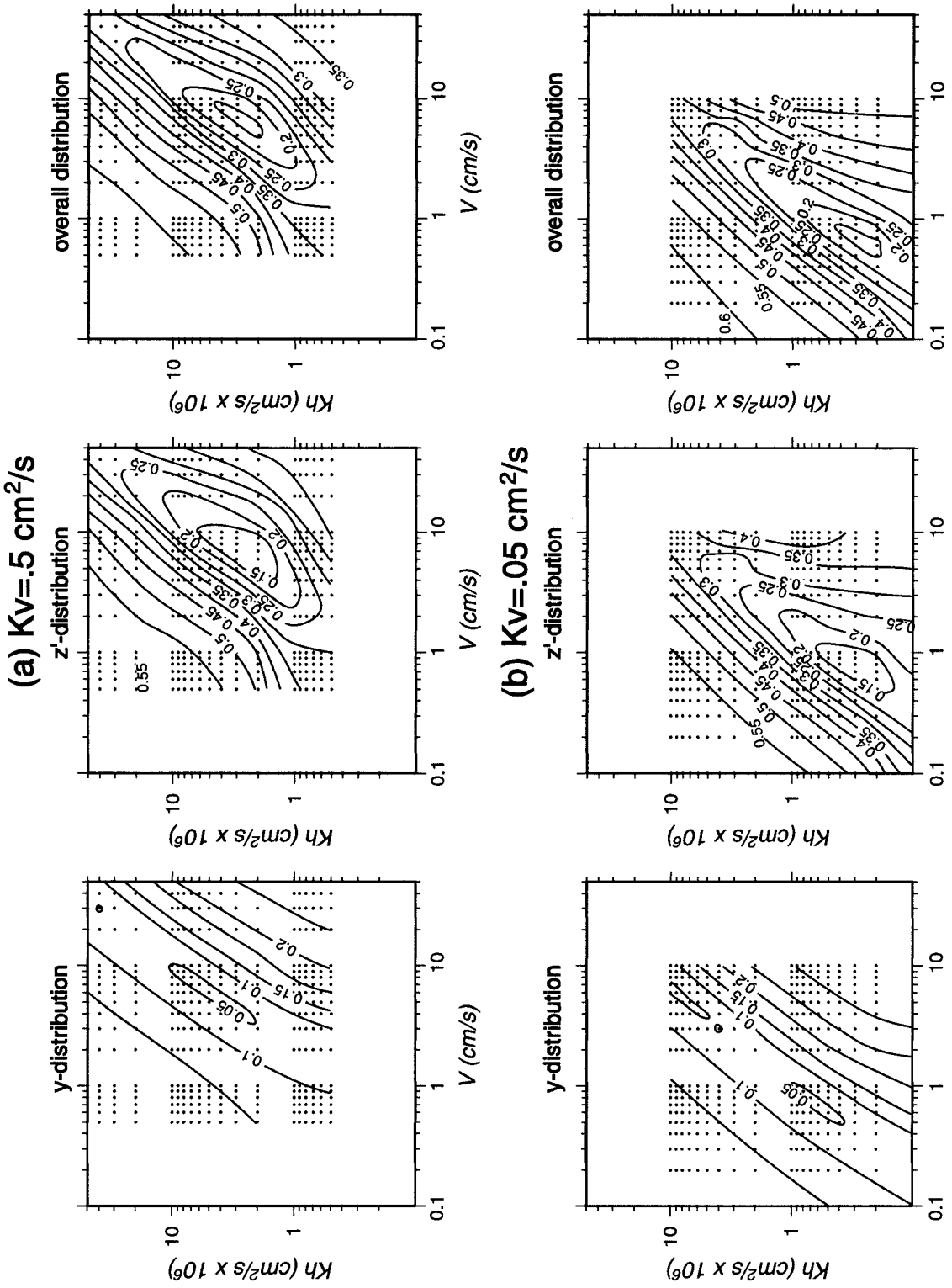

FIG. 13. Rms fit of the model solution to the observed distribution of accumulated temperature change for two different choices of diapycnal mixing (top row $\kappa_v = 0.5$ cm^2 s^{-1}, bottom row $\kappa_v = 0.05$ cm^2 s^{-1}). The optimal fit is indicated by the minimum in rms for the cross-stream distribution (left), vertical distribution (center), and the overall distribution in a vector sense (right).

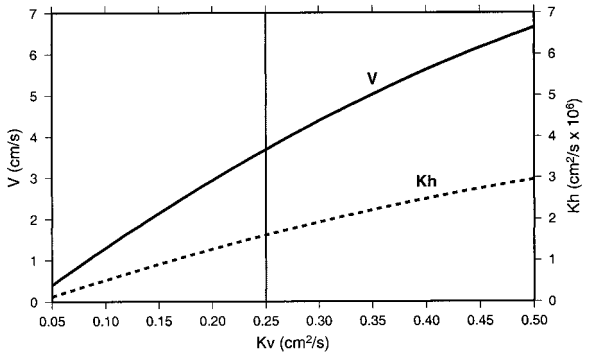

FIG. 14. Optimal pumping speed and isopycnal diffusivity for different values of the diapycnal diffusivity. The best choice implied by the observations is indicated by the gray line.

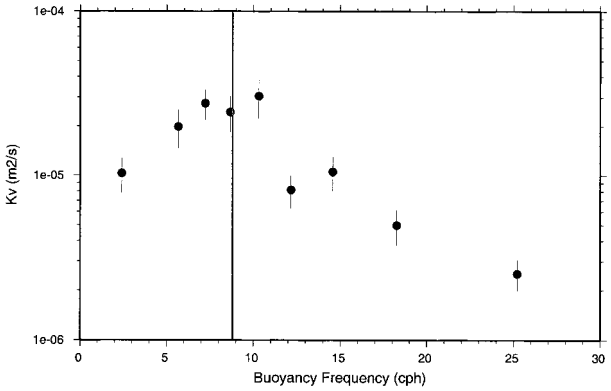

FIG. 15. Measured values of diapycnal mixing from the CMO experiment, reported by Rehmann and Duda (2000) (uncertainties are indicated by the thin vertical lines). The value of buoyancy frequency observed in the detached BBL is marked by the gray line.

6. Secondary circulation

a. Detachment mechanisms

It is enlightening to compare the path of the detached BBL, as determined by the accumulated temperature change, to the flow field measured by the shipboard ADCP. As mentioned in section 2 the ADCP velocities have been corrected for the barotropic tide, and, according to moored measurements in the shelfbreak jet along the TOPEX line, the baroclinic tides and inertial motions are small (FPTS). The velocity fields have been rotated into a stream coordinate system, where the along-stream direction is determined by the mean transport vector of the jet (see FPTS for a detailed discussion of the methodology used). To leading order the flow is along the isobaths, and positive x, u denote equatorward distance and velocity, while positive y, v are directed offshore. The alongstream ADCP section reveals a strong shelfbreak jet (u order 30 cm s^{-1}) whose high velocity core bends shoreward with depth and extends to the bottom (Fig. 17a). Note the flow reversal aligned directly beneath the surface signature of the jet (near $y = 115$ km); this feature is similar to the geostrophically adjusted jet of Chapman and Lentz (1994). The section of cross-stream velocity reveals a region of strong convergence (v order 15 cm s^{-1}) located in the lower part of the jet (Fig. 17b). Both the alongstream and cross-stream jet structure seen in Fig. 17 are reminiscent of the mean jet features presented by Fratantoni et al. using the full collection of PRIMER shipboard ADCP sections. Note that the position of the jet and the associated shelfbreak front (particularly the grounding of the front, Fig. 17c) implies a dynamical significance to the mini-shelfbreak located near 105 km. In fact, plotted as such, one would easily mistake this to be a jet overlying the shelfbreak proper.

The path of the detached BBL is even better understood when viewed in light of the velocity and density structure of the shelfbreak jet (see the overlays in Fig. 17). The tongue of accumulated temperature change emanates at the foot of the front (Fig. 17c) and abuts the line of zero cross-stream velocity as it progresses through the water column (onshore flow inhibits any further seaward penetration of the BBL tongue, Fig. 17b). The dynamics dictating the detachment are thus consistent with those expounded by Gawarkiewicz and Chapman (1992), whereby a strong adverse pressure

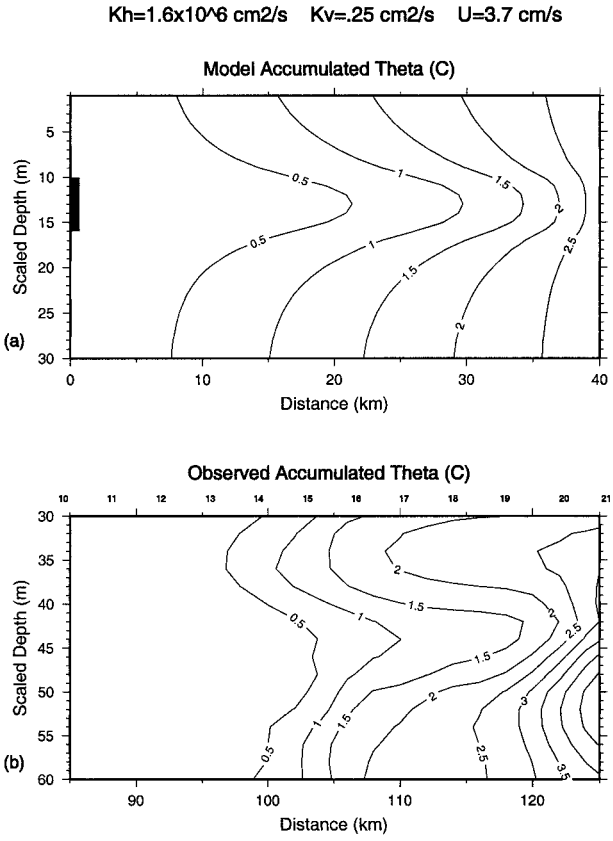

FIG. 16. (a) Modeled accumulated temperature change for the best choice of parameters (see Fig. 14) compared to (b) observed tongue of accumulated temperature change.

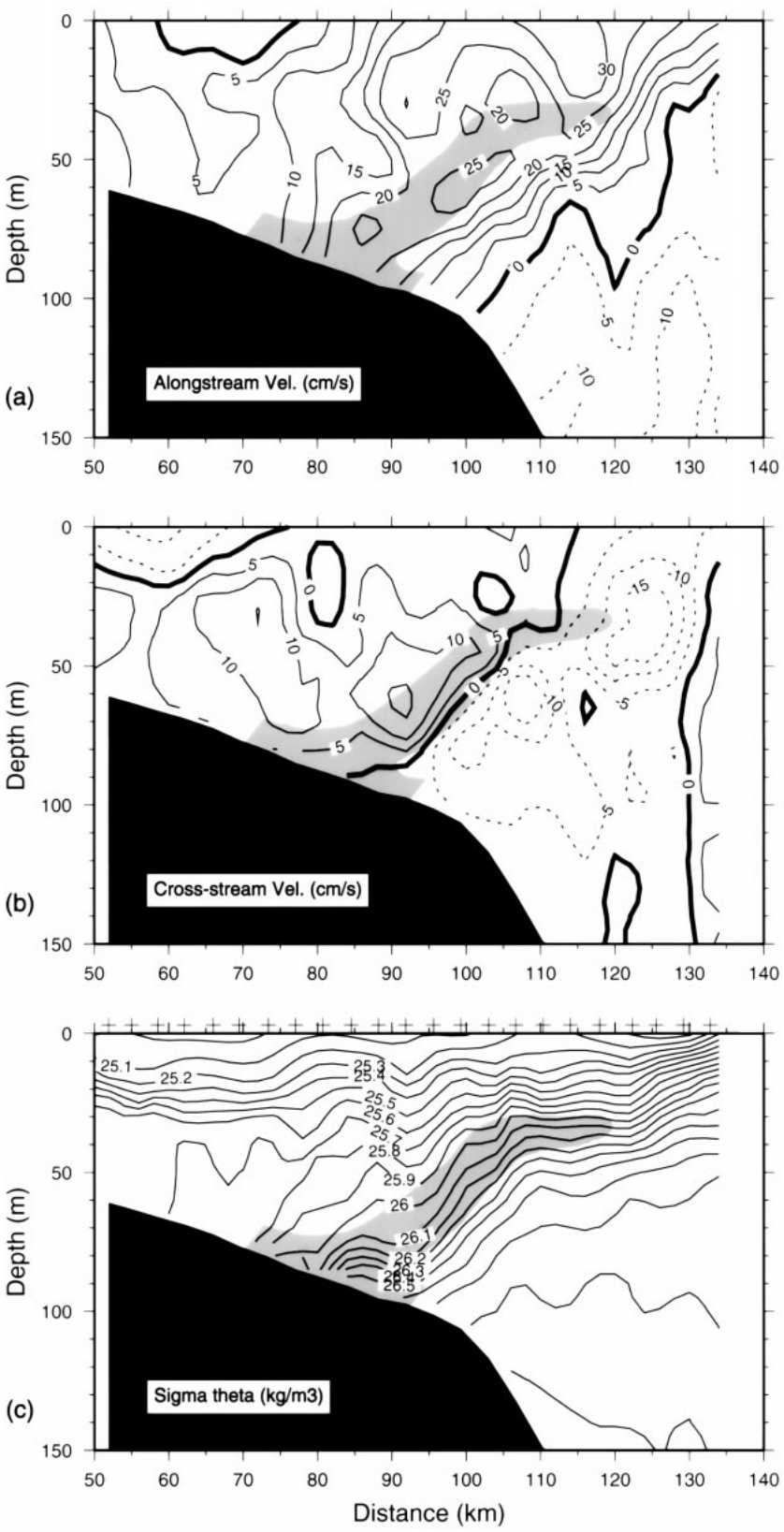

FIG. 17. ADCP velocity fields and the CTD density field, overlayed by the path of the detached BBL (i.e., the tongue of accumulated temperature change from Fig. 10, denoted by gray shading).

gradient is set up by the concentration of frontal isopycnals at the bottom.

It is worth noting that the two patches of dye analyzed by Houghton and Visbeck (1998) were most likely released a bit seaward of the tongue of accumulated temperature change seen in Fig. 17. This is evident by the fact that, when the dye upwelled out of the BBL, it entered the (bottom portion of the) highly stratified foot of the front. In the CTD section presented here the analogous location would be close to station 10 or 11 (see Fig. 7). Recall that the detached BBL in Fig. 7 is bounded at the bottom by the (top portion of the) front. Hence according to these results the initial dye streaks were positioned a bit downslope of the region of strongest detachment. By contrast the dye patch analyzed by Houghton (1997) did not upwell, but remained within the BBL as it progressed upslope. Houghton (1997) attributed this to the mechanism of Chapman and Lentz (1994). The results presented here support this claim and suggest that, in the context of the present observations, the initial streak was released within the flow reversal in Fig. 17a (where the BBL advection would be upslope).

b. Interior circulation cell

The strong cross-stream convergence of the jet at depth suggests that some of the interior convergent flow may upwell and enhance the flow of the detached BBL. Barth et al. (1998) observed a similar situation and computed the corresponding vertical velocity, assuming (arbitrarily) that all of the cross-stream flow upwelled. The same assumption here results in unrealistically large upwelling. Note in Fig. 2b that the PRIMER CTD section is located in an area where the isobaths are convergent (e.g., note the region between the 80 m and 150 m isobaths from 69°55′W to the TOPEX line). For a jet that extends to the bottom, as is observed here, one would expect significant cross-stream convergence simply due to alongstream continuity in the transport of the jet. The convergence implied by the isobath configuration in Fig. 2, for a jet speed of 25 cm s^{-1}, is enough to account for half of the observed cross-stream convergence in Fig. 17b. It is thus assumed that the remaining convergence results in upwelling.

In their analysis Barth et al. (1998) assumed $w = 0$ at the bottom, then integrated the continuity equation to estimate the upwelling, $w = \int (dv/dy)\, dz$. This resulted in their estimate of 9 m day^{-1}, which they likened to the value obtained by the dye-release of Houghton and Visbeck (1998). However, this may be an unfair comparison as it is unclear if the dye is upwelling due to the detached BBL or due to subsequent cross-stream convergence in the interior (or both). To address this issue here, the bottom boundary condition for w was carefully considered. According to theory for an (unstratified) Ekman layer on a sloping bottom (Pedlosky 1979), the bottom boundary condition for the interior vertical velocity is

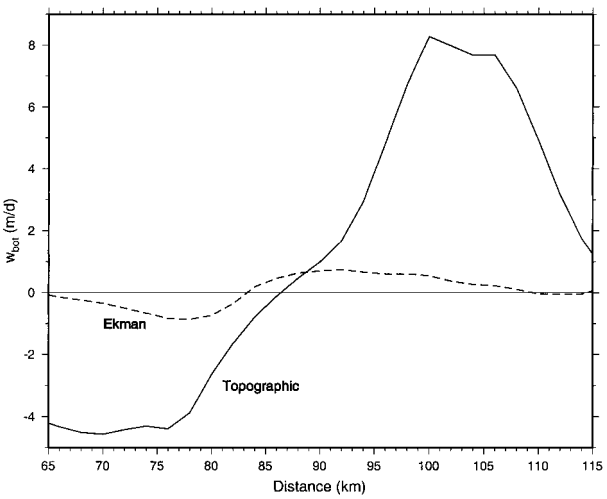

FIG. 18. The two contributions to the vertical velocity [see Eq. (4)], used as the bottom boundary condition for computing the secondary circulation.

$$w_{\text{bot}} = \left(\frac{\delta_E}{2}\right)\frac{du}{dy} + v\alpha, \tag{4}$$

where $\delta_E = (2\nu/f)^{1/2}$ is the Ekman depth, ν is the vertical viscosity, f is the Coriolis parameter, and α is the bottom slope. The first term in this expression is the Ekman pumping, and the second is the inviscid condition of no flow normal to the boundary. Both terms can be estimated using the data. However, because of the near-bottom blanking region of the ADCP measurements (extending 15–20 m above the bottom in the vicinity of the front), it was necessary to use extrapolated values of u and v. Two-dimensional Laplacian-spline gridding was applied to both the along- and cross-stream ADCP sections, which resulted in straightforward extrapolation due to the deep-reaching extension of the jet (see Figs. 17a and 17b). A value of 1 cm^2 s^{-1} was used for the vertical viscosity, and the bottom slope was determined from the chirp sonar data. The calculation of (4) was restricted to ± 25 km on either side of the jet.

The result (albeit for an unstratified flow) suggests that w_{bot} is dominated by the inviscid component, though both components show a similar cross-stream trend (Fig. 18). Positive Ekman pumping occurs throughout the frontal region, comparable in magnitude to that found in the Chapman and Lentz (1994) model. The reason for the strong positive topographic component is the significant onshore velocity in conjunction with the steepness of the mini-shelfbreak. Taking w_{bot} as the bottom boundary condition, the interior vertical velocity w was then obtained via the continuity equation. It is assumed here that half of the cross-stream convergence dv/dy is feeding the alongstream acceleration of the jet, in line with the argument above. (It should be noted

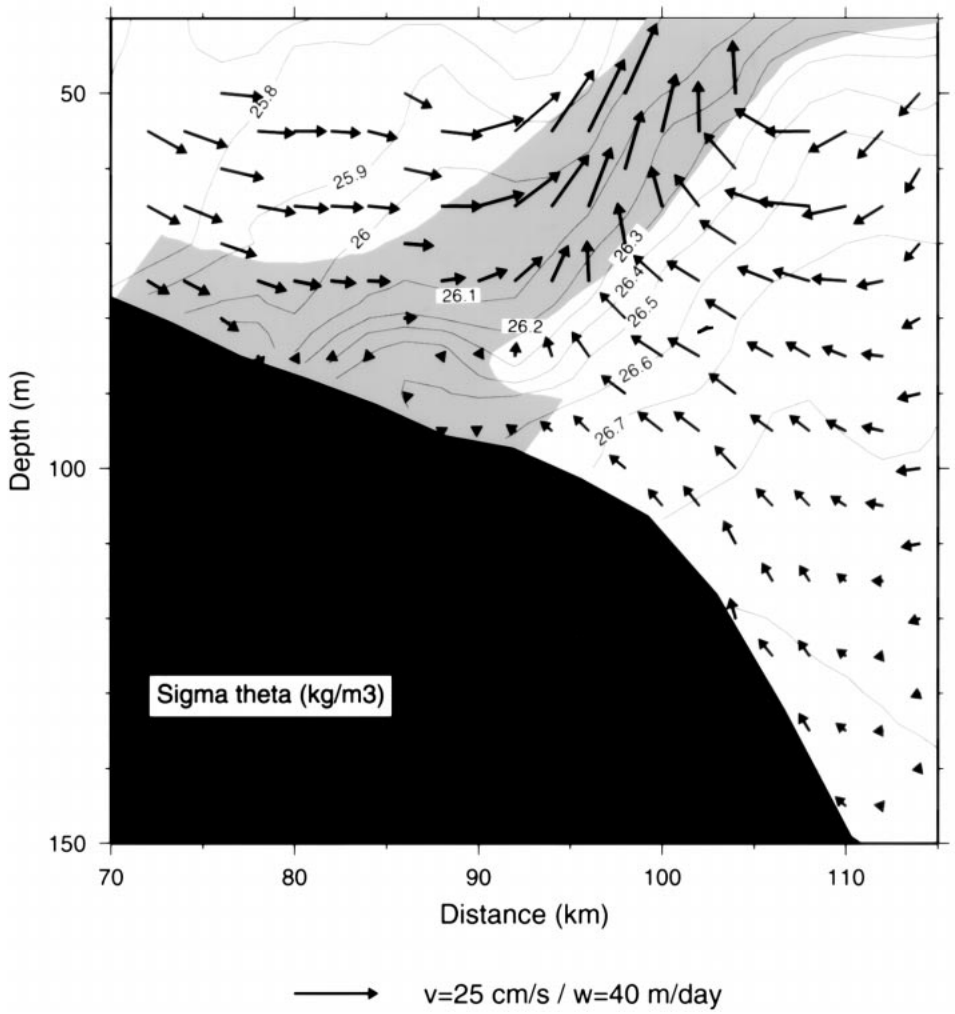

FIG. 19. Inferred secondary circulation (vectors) in relation to the density field and detached BBL (gray shading).

that to compute dv/dy a low-pass filter was invoked due to the inherent noise in this quantity.) Finally, combining w with the cross-stream velocity v, the circulation in the cross-stream plane was determined for the lower part of the water column.

The secondary circulation in the PRIMER hydrographic section shows a robust deep cell associated with the shelfbreak jet (Fig. 19). The strongest flow is aligned along the detached BBL, which helps to explain why the tongue of accumulated temperature change is so pronounced. At first glance this cell appears similar to the one found in the Chapman and Lentz (1994) model. However, the convergence in their cell occurs only within the BBL, and the cell then extends the entire width of the water column with corresponding divergence near the surface. Furthermore, the strength of their cell is an order of magnitude weaker than that observed here, despite the fact that the jet is of similar strength [keep in mind that there is no ambient stratification in the Chapman and Lentz (1994) model]. By contrast, the secondary cell observed here is largely an interior feature. It arises predominantly from the strong deep convergence in the jet (i.e., above the BBL), which is likely related to the topography in the region. Recall that the advective–diffusive model predicted a pumping speed of 3.7 cm s^{-1} along the detached BBL, which translates to an upwelling of 9 m day^{-1}. The average observed upwelling along this layer from Fig. 19 is 23 m day^{-1}, larger by a factor of 2. Based on the fact that the tracer estimate is an average in both time and space and noting the uncertainty in the observed diapycnal diffusivity, the agreement is reasonable.

Although the upwelling in Fig. 19 is mostly due to interior convergence [and not solely an extension of the flow emanating from the BBL as in the Chapman and Lentz (1994) model], this is likely not always the case in the Middle Atlantic Bight shelfbreak jet. At a different time or location the flow could very well be predominantly derived from the BBL, though the resulting secondary cell would clearly be weaker [in line with

Chapman and Lentz's (1994) results]. The Houghton and Visbeck (1998) dye release estimate of 4 m day^{-1} is presumably a direct measure of such BBL pumping, whereas Barth et al.'s (1998) upwelling rate applies to the interior. In any event, the property tongue observed in the PRIMER CTD section indicates a nontrivial contribution from the BBL in a space/time averaged sense.

Finally, it is worth commenting on the mass balance implied by these observations, assuming that the jet is accelerating throughout the water column by the amount required by the isobath configuration. Note the pattern of cross-stream velocity aligned with the axis of the jet (Fig. 17b): strong deep convergence, little to no convergence at middepth, and moderate convergence near the surface. As discussed above, dv/dy feeds the alongstream acceleration of the deep portion of the jet, with the remainder resulting in upwelling. Farther up in the water column, however, the near-zero dv/dy is not sufficient for this, implying that dw/dz must balance du/dx at middepth. This is approximately enough to bring w to zero, thus ''closing'' the secondary circulation cell at middepth, that is, beneath the seasonal pycnocline. Finally, in the upper layer the moderate dv/dy is the correct magnitude to balance the alongstream acceleration.

Hence, the observed secondary circulation cell of Fig. 19 is made complete by envisioning the flow vectors turning out of the page at middepth. While this scenario satisfies the three-dimensional mass balance, there are certainly unresolved issues. One of these is the evolution of density following water parcels in the cell. To leading order the shoreward side of the cell is isopycnal. However, the flow on the seaward side is either entrained into the front, implying strong diapycnal mixing in this region, or the flow is advecting the front seaward. It would be of interest to consider such scenarios in future experiments.

7. Summary

Analysis of a synoptic hydrographic/velocity crossing of the shelfbreak jet in the Middle Atlantic Bight has shed light on the character and dynamics of the bottom boundary layer (BBL). The cross-stream distribution of BBL properties shows a distinct change in the vicinity of the front. Specifically, the BBL thins, becomes more stratified, and is separated from the interior by a stronger density cap. Coincident with this are changes in the overlying interior flow, which is both stronger in this region and more strongly stratified. According to previous models, stronger equatorward flow of the jet should result in a larger BBL thickness, contrary to these observations. This implies that the interior stratification has stronger influence on the BBL (models have not yet addressed the case of horizontally varying interior stratification). A second thinning of the BBL occurs just prior to the shelfbreak. This is aligned with a local minimum in bottom slope and with the presence of a near-bottom lens of cold, fresh slope water.

Where the BBL first thins on the shoreward edge of the front, it, in fact, briefly disappears altogether. Detailed analysis of the θ, S data shows that the BBL detaches at this location and spreads into the interior along an (nearly) isopycnal layer abutting the front. This layer is characterized by weak vertical stratification, bounded at the top by the same density cap present in the BBL and at the bottom by the front itself. The layer is further identified by anomalously weak along-isopycnal gradients of θ and S due to the pumping of water parcels along the layer. This interpretation is supported by the results of an advective–diffusive model of the detachment, which produces a tongue of minimum accumulated temperature change along the layer in line with that observed in the hydrographic section. Using measured values of diapycnal diffusivities from a nearby site, the model output was tuned to the observations, producing a pumping estimate of 3.7 cm s^{-1} and an along-isopycnal diffusivity of 1.6×10^6 cm^2 s^{-1}.

The velocity fields from the shipboard ADCP revealed that at the time of the crossing the jet extended to the bottom, with a flow reversal just seaward of this. The jet itself was characterized by strong, deep cross-stream convergence. Since the detached BBL tracks the line of maximum interior convergence, this suggests that upwelling resulting from the cross-stream convergence might contribute to the flow along the layer. This was investigated by calculating the vertical velocity, via the continuity equation, under the assumption that the jet is accelerating locally due to the convergent isobaths. The bottom boundary condition for w was determined as the sum of the Ekman pumping in the BBL and the topographic component due to a sloping bottom (of which the latter is significantly stronger). The secondary circulation so calculated reveals a clearly defined deep cell with a concentration of flow along the detached BBL, clearly demonstrating that (at this location and time) the detached BBL is significantly enhanced by interior convergence. Mass balance considerations implies that this cell must be three-dimensional and is confined to middepth.

These results have demonstrated that the dynamics of bottom boundary layer detachment, suggested by the models of Gawarkiewicz and Chapman (1992) and Chapman and Lentz (1994), are likely at work in the Middle Atlantic Bight. The detached BBL observed in the hydrographic section occurs near the concentration of isopycnals associated with the foot of the shelfbreak front, implicating the importance of the adverse pressure gradient discussed by Gawarkiewicz and Chapman (1992). Among the aspects that future models need to consider are variable ambient stratification and alongstream variation in topography—both of which are likely of fundamental importance in the Middle Atlantic Bight. Finally, the results presented here are consistent with the observations of Houghton and Visbeck (1998) and

Barth et al. (1998) who also detected detachment of the BBL in the shelfbreak jet. A unique aspect of the present study is that it invoked only the basic temperature and salinity data, and hence is applicable to historical hydrographic sections.

Acknowledgments. Much assistance was received throughout the course of this work from numerous people. Daniel Torres, Paula Fratantoni, and Alberto Scotti together produced the detided shipboard ADCP data. Terry McKee processed the CTD dataset, and Sarah Zimmermann helped interpret it. Glen Gawarkiewicz helped motivate the work, and provided valuable input at every stage of it. Finally, discussions with Steve Lentz and Dave Chapman resulted in clearer presentation of the results. This work was funded by ONR Contract N00014-98-10046 as part of the Shelfbreak PRIMER experiment.

REFERENCES

Barth, J. A., D. Bogucki, S. D. Pierce, and P. M. Korso, 1998: Secondary circulation associated with a shelfbreak front. *Geophys. Res. Lett.,* **25,** 2761–2764.

Chapman, D. C., and S. J. Lentz, 1994: Trapping of a coastal density front by the bottom boundary layer. *J. Phys. Oceanogr.,* **24,** 1464–1479.

——, and ——, 1997: Adjustment of stratified flow over a sloping bottom. *J. Phys. Oceanogr.,* **27,** 341–356.

Garrett, C., P. MacCready, and P. Rhines, 1993: Boundary mixing and arrested Ekman layers: Rotating stratified flow near a sloping boundary. *Annu. Rev. Fluid Mech.,* **25,** 291–323.

Gawarkiewicz, G. G., and D. C. Chapman, 1992: The role of stratification in the formation and maintenance of shelf-break fronts. *J. Phys. Oceanogr.,* **22,** 753–772.

Houghton, R., 1997: Lagrangian flow at the foot of a shelfbreak front using a dye tracer injected into the bottom boundary layer. *Geophys. Res. Lett.,* **24,** 2035–2038.

——, and M. Visbeck, 1998: Upwelling and convergence in the Middle Atlantic Bight shelf break front. *Geophys. Res. Lett.,* **25,** 2765–2768.

Linder, C. A., and G. G. Gawarkiewicz, 1998: A climatology of the shelfbreak front in the Middle Atlantic Bight. *J. Geophys. Res.,* **103,** 18 405–18 423.

Loder, J., B. Petrie, and G. Gawarkiewicz, 1998: The coastal ocean off northeastern North America: A large scale view. *The Sea.* Vol. 11: *The Global Ocean Regional Studies and Syntheses,* A. Robinson and K. Brink, Eds., 105–133.

MacCready, P., and P. B. Rhines, 1993: Slippery bottom boundary layers on a slope. *J. Phys. Oceanogr.,* **23,** 5–22.

Middleton, J. F., and D. Ramsden, 1996: The evolution of the bottom boundary layer on the sloping continental shelf: A numerical study. *J. Geophys. Res.,* **101,** 18 061–18 077.

Pedlosky, J., 1979. *Geophysical Fluid Dynamics.* Springer-Verlag, 624 pp.

Pickart, R. S., and W. M. Smethie Jr., 1998: Temporal evolution of the Deep Western Boundary Current where it enters the subtropical domain. *Deep-Sea Res.,* **45,** 1053–1083.

——, D. J. Torres, T. K. McKee, M. J. Caruso, and J. E. Przystup, 1999: Diagnosing a meander of the shelfbreak current in the Middle Atlantic Bight. *J. Geophys. Res.,* **104,** 3121–3132.

Rehmann, C. R., and T. F. Duda, 2000: Diapycnal diffusivity inferred from scalar microstructure measurements near the New England shelf/slope front. *J. Phys. Oceanogr.,* **30,** 1354–1371.

Stahr, F. R., and T. B. Sanford, 1999: Transport and bottom boundary layer observations of the North Atlantic deep western boundary current at the Blake Outer Ridge. *Deep-Sea Res.,* **46,** 205–243.

Trowbridge, J. H., and S. J. Lentz, 1991: Asymmetric behavior of an oceanic boundary layer above a sloping bottom. *J. Phys. Oceanogr.,* **21,** 1171–1185.

——, and ——, 1998: Dynamics of the bottom boundary layer on the northern California shelf. *J. Phys. Oceanogr.,* **28,** 2075–2093.